APPLIED GEOPHYSICS, Vol.11, No.2 (June 2014), P. 186-196, 12 Figures.
DOI: 10.1007/s11770-014-0431-7

Multiwave velocity analysis based on Gaussian beam prestack depth migration

Han Jian-Guang[1,2], Wang Yun[3♦], Han Ning[4], Xing Zhan-Tao[1], and Lu Jun[5]

Abstract: Prestack depth migration of multicomponent seismic data improves the imaging accuracy of subsurface complex geological structures. An accurate velocity field is critical to accurate imaging. Gaussian beam migration was used to perform multicomponent migration velocity analysis of PP- and PS-waves. First, PP- and PS-wave Gaussian beam prestack depth migration algorithms that operate on common-offset gathers are presented to extract offset-domain common-image gathers of PP- and PS-waves. Second, based on the residual moveout equation, the migration velocity fields of P- and S-waves are updated. Depth matching is used to ensure that the depth of the target layers in the PP- and PS-wave migration profiles are consistent, and high-precision P- and S-wave velocities are obtained. Finally, synthetic and field seismic data suggest that the method can be used effectively in multiwave migration velocity analysis.
Keywords: Gaussian beam migration; multiwave; migration velocity analysis; common-image gathers

Introduction

The method of prestack depth migration for multicomponent seismic data improves the imaging accuracy of reservoirs and other complex geological structures (Du et al., 2012). High-quality migration imaging of multicomponent seismic data depends not only on the multiwave migration algorithm but also on the accuracy of the P- and S-wave migration velocity models. Therefore, in addition to studying the multiwave migration algorithm, obtaining accurate P- and S-wave migration velocities has become an important research topic. In this study, migration velocity analysis is used to iteratively update and construct the velocity model. The error is highly sensitive to the velocity model and it is estimated after the depth migration.

Presently, residual curvature analysis (RCA) is commonly used in migration velocity analysis. Al-Yahya (1989) first proposed this approach based on common-image gathers (CIGs) and applied it to horizontal reflectors. Later, Lee and Zhang (1992) derived a dip-

Manuscript received by the Editor December 26, 2013; revised manuscript received May 19, 2014
*This research was supported by the National Special Fund of China (No. 2011ZX05035-001-006HZ, 2011ZX05008-006-22, 2011ZX05049-01-02, and 2011ZX05019-003), the National Natural Science Foundation of China (No. 41104084), and the PetroChina Innovation Foundation (No. 2011D-5006-0303).
1 Institute of Geology and Geophysics, Chinese Academy of Sciences, Beijing 100029, China.
2 University of Chinese Academy of Sciences, Beijing 100049, China.
3 Institute of Geochemistry, Chinese Academy of Sciences, Guiyang 550002, China.
4 College of Resources and Environment, Southwest University, Chongqing 400716, China.
5 China University of Geosciences (Beijing), Beijing 100083, China.
♦Corresponding Author: Wang Yun (E-mail: yunwang@mail.iggcas.ac.cn)

corrected residual moveout equation for small-angle dip reflectors. To handle complex structures, Lanford and Levander (1993) proposed an RCA method based on the layer-stripping algorithm. They assumed that the medium consisted of constant-velocity layers, and the velocity along the ray path was updated as in tomographic reconstruction. Liu and Bleistein (1994, 1995) and Liu (1997) quantitatively described the relationship between migration imaging and migration velocity, and then derived a general residual moveout representation that is valid for any velocity distribution and any subsurface structure.

Recently, angle-domain common-image gathers using the wave equation migration in migration velocity analysis have been discussed by several authors (Sava and Biondi, 2004a, b; Sava et al., 2005). In light of the developments in multicomponent seismic technology, converted wave migration velocity analysis methods have been proposed. Liu (1995) extended the perturbation method of P-waves to converted waves and presented a formula for the analysis of the converted wave migration velocity. Maria and Robert (1998) derived the relationship between residual moveout in converted wave CIGs and residual velocity based on perturbation theory. Dai and Li (2005, 2007) proposed an approach for updating the velocity model in prestack Kirchhoff time migration of converted waves. Yan and Sava (2010) studied the wave equation migration velocity for converted waves in the depth domain.

In these methods, greater accuracy in migration velocity analysis is achieved based on the time-consuming wave equation migration method. Velocity analysis based on Kirchhoff migration is more efficient because it does not require output for every CIG; however, CIGs usually produce artifacts due to multipathing, which affect the quality of the migration velocity analysis. Gaussian beam migration (Hale, 1992a, b; Hill, 1990, 2001; Gray, 2005; Gray and Bleistein, 2009; Nowack et al., 2010; Popov et al., 2010) is an elegant and efficient depth migration method with accuracy comparable to the wave equation migration and flexibility comparable to Kirchhoff migration. It can also solve for multivalued travel times with different superposed beams. However, Gaussian beam migration studies have mainly focused on acoustic wave migration and generally neglected migration velocity analysis.

This study discusses multicomponent migration velocity analysis for PP- and PS-waves based on Gaussian beam prestack depth migration. The goal is to propose an effective method for obtaining accurate P- and S-wave migration velocities for high-quality multicomponent seismic data migration imaging.

Common-image gathers based on Gaussian beam migration

The local slant stack is the principal algorithm in the Gaussian beam migration method, which decomposes a certain range of seismic records near the beam center into different outgoing directional local plane waves for wave field extrapolation. Because the beam center spacing is several times greater than the receiver spacing is, and beam center spacing is relatively sparse, it is difficult to extract the offset-domain common-image gathers (ODCIGs) using the common-shot Gaussian beam prestack depth-migration algorithm. Thus, in this study, ODCIGs are generated by the Gaussian beam prestack depth migration method that operates on common-offset gathers.

Gaussian beam prestack migration theory

In multicomponent seismic exploration, the Z- and X-component records receive part of the PS- and PP-waves but not the pure PP- and PS-waves. Direct use of the Z- and X-components to migrate will produce wave field crosstalk in the migration profiles. Thus, we first separate the PP- and PS-waves from the multicomponent seismic data using a wave vector rotation transformation method in an affine coordinate system (Lu et al., 2012) that recovers the true amplitude of the PP- and PS-waves to obtain genuine pure PP- and PS-waves, unlike traditional wave-separation methods that use a Cartesian reference system. Second, the multicomponent Gaussian beam prestack depth migration imaging conditions for the PP- and PS-waves are presented.

A prestack migration image of the Gaussian beam is formed by cross-correlating the downward-continued wave fields from the source and beam centers. In a two-dimensional isotropic medium, we assume that $\mathbf{x}_s=(x_s, 0)$ and $\mathbf{x}_r=(x_r, 0)$ denote the source and receiver locations, respectively. According to the Gaussian beam prestack migration method that operates on the common-offset gathers of Hill (2001), the PP- and PS-wave common-offset gathers for Gaussian beam migration may be written as

$$I^{PP}(\mathbf{x}) = -\frac{2}{\pi}\int d\omega \int dx_h \int dx_m \frac{\partial G^{P*}(\mathbf{x},\mathbf{x}_s,\omega)}{\partial z_s}\frac{\partial G^{P*}(\mathbf{x},\mathbf{x}_r,\omega)}{\partial z_r}u^{PP}(\mathbf{x}_h,\mathbf{x}_m,\omega), \quad (1)$$

$$I^{PS}(\mathbf{x}) = -\frac{2}{\pi}\int d\omega \int dx_h \int dx_m \frac{\partial G^{P*}(\mathbf{x},\mathbf{x}_s,\omega)}{\partial z_s}\frac{\partial G^{S*}(\mathbf{x},\mathbf{x}_r,\omega)}{\partial z_r} u^{PS}(\mathbf{x}_h,\mathbf{x}_m,\omega), \tag{2}$$

where $I^{PP}(\mathbf{x})$ and $I^{PS}(\mathbf{x})$ are PP- and PS-wave final images at the subsurface point $\mathbf{x}=(x,z)$, respectively, ω is the circular frequency, *denotes the complex conjugate, $u^{PP}(\mathbf{x}_h,\mathbf{x}_m,\omega)$ and $u^{PS}(\mathbf{x}_h,\mathbf{x}_m,\omega)$ are the recorded wave fields of the PP- and PS-waves at half offset, respectively, $\mathbf{x}_h = (x_h,0)$ and mid-point $\mathbf{x}_m = (x_m,0)$, $G^P(\mathbf{x},\mathbf{x}_s,\omega)$ is the P-wave Green's function for the source, and $G^P(\mathbf{x},\mathbf{x}_r,\omega)$ and $G^S(\mathbf{x},\mathbf{x}_r,\omega)$ are the P- and S-wave Green's function for the receiver, respectively.

The source and receiver positions can be changed to mid-point and the half-offset coordinates using the equation $\mathbf{x}_m = \mathbf{x}_r - \mathbf{x}_h = \mathbf{x}_s + \mathbf{x}_h$. The beam center position $\mathbf{L}_m = (L_m,0)$ is calculated in common-offset gathers, and Green's function for the source and receiver near-beam center point $\mathbf{L}_m$ are constructed with Gaussian beams from the $\mathbf{L}_m - \mathbf{x}_h$ and $\mathbf{L}_m + \mathbf{x}_h$ positions, respectively. These steps result in

$$\mathrm{G}(\mathbf{x},\mathbf{x}_s,\omega) \approx \frac{i}{2\pi}\int \frac{dp_{sx}}{p_{sz}} \mathrm{u}_{GB}(\mathbf{x},\mathbf{L}_m - \mathbf{x}_h,\mathbf{p}_s,\omega)\exp[-i\omega p_{sx}(x_m - L_m)], \tag{3}$$

$$\mathrm{G}(\mathbf{x},\mathbf{x}_r,\omega) \approx \frac{i}{2\pi}\int \frac{dp_{rx}}{p_{rz}} \mathrm{u}_{GB}(\mathbf{x},\mathbf{L}_m + \mathbf{x}_h,\mathbf{p}_r,\omega)\exp[-i\omega p_{rx}(x_m - L_m)], \tag{4}$$

where $\mathbf{P}_s = (p_{sx},p_{sz})$ and $\mathbf{P}_r = (p_{rx},p_{rz})$ are the source and receiver ray parameter vectors, respectively, and $\mathrm{u}_{GB}(\mathbf{x},\mathbf{x_0},\mathbf{p},\omega)$ is the Gaussian beam solution to the wave equation (Červeny et al., 1982; Nowack, 2003). If functions A and T represent the complex amplitude and travel time of the Gaussian beam, the Gaussian beam expression is

$$\mathrm{u}_{GB}(\mathbf{x},\mathbf{x_0},\mathbf{p},\omega) = A\exp(i\omega T). \tag{5}$$

Gaussian beam expressions have the same form for P- and S-waves. The only difference is the corresponding P- and S-wave velocities required in the calculation (Červeny, 1983). Therefore the Green's function in terms of Gaussian beams can be used to describe the P- and S-wave components (Nowack et al., 2006; Nowack et al., 2007). Green's function constructed from Gaussian beams is the summation of the local wave field limited to the area near the central rays. It can be used to solve for multivalued travel times with different superposed beams (Hill, 2001). Therefore, a multiwave migration velocity analysis method based on Gaussian beam migration effectively eliminates the artifacts in common-image gathers due to multivalued travel times and improves the accuracy of the migration velocity analysis.

Inserting the P- and S-waves Green's function into equations (1) and (2) transforms them to

$$I^{PP}(\mathbf{x}) = C^{PP}\int dx_h \sum_{L_m}\int d\omega D^{PP}(\mathbf{L}_m,\mathbf{p}_m^{PP},\omega) \times \int dp_{mx}^{PP}\int dp_{hx}^{PP}\overline{A}^{PP}(\mathbf{x},\mathbf{p}_m^{PP},\mathbf{p}_h^{PP})\exp\left[-i\omega\overline{T}^{PP}(\mathbf{x},\mathbf{p}_m^{PP},\mathbf{p}_h^{PP})\right], \tag{6}$$

$$I^{PS}(\mathbf{x}) = C^{PS}\int dx_h \sum_{L_m}\int d\omega D^{PS}(\mathbf{L}_m,\mathbf{p}_m^{PS},\omega) \times \int dp_{mx}^{PS}\int dp_{hx}^{PS}\overline{A}^{PS}(\mathbf{x},\mathbf{p}_m^{PS},\mathbf{p}_h^{PS})\exp\left[-i\omega\overline{T}^{PS}(\mathbf{x},\mathbf{p}_m^{PS},\mathbf{p}_h^{PS})\right], \tag{7}$$

where C^{PP} and C^{PS} are corresponding constants and $\mathbf{P}_m$ and $\mathbf{P}_h$ are the mid-point and offset ray parameter vectors, respectively, which are equivalent to the identifying source and receiver ray parameter vectors. For PP- and PS-waves, the expressions are

$$\mathbf{p}_m^{PP} = \mathbf{p}_s^P + \mathbf{p}_r^P, \tag{8}$$

$$\mathbf{p}_m^{PS} = \mathbf{p}_s^P + \mathbf{p}_r^S, \tag{9}$$

where $D^{PP}(\mathbf{L}_m, \mathbf{p}_m^{PP}, \omega)$ and $D^{PS}(\mathbf{L}_m, \mathbf{p}_m^{PS}, \omega)$ are the local plane wave components of PP- and PS-waves, respectively, obtained from the local slant stack of the common-offset traces. D^{PP} and D^{PS} are expressed as

$$D^{PP}(\mathbf{L}_m,\mathbf{p}_m^{PP},\omega) = \frac{1}{4\pi^2}\left|\frac{\omega}{\omega_r}\right|^3 \int dx_m u^{PP}(\mathbf{x}_h,\mathbf{x}_m,\omega) \times \exp\left[-i\omega P_{mx}^{PP}(x_m - L_m) - \frac{1}{2}\left|\frac{\omega}{\omega_r}\right|\frac{|x_m - L_m|^2}{L_0^2}\right], \tag{10}$$

$$D^{PS}(\mathbf{L}_m,\mathbf{p}_m^{PS},\omega) = \frac{1}{4\pi^2}\left|\frac{\omega}{\omega_r}\right|^3 \int dx_m u^{PS}(\mathbf{x}_h,\mathbf{x}_m,\omega) \times \exp\left[-i\omega P_{mx}^{PS}(x_m - L_m) - \frac{1}{2}\left|\frac{\omega}{\omega_r}\right|\frac{|x_m - L_m|^2}{L_0^2}\right], \tag{11}$$

where L_0 is the initial beam width at the reference frequency ω_r. The local slant stack transform effectively improves the computational efficiency of the migration.

In common-offset gathers, $\overline{A}^{PP}(\mathbf{x}, \mathbf{p}_m^{PP}, \mathbf{p}_h^{PP})$ and $\overline{T}^{PP}(\mathbf{x}, \mathbf{p}_m^{PP}, \mathbf{p}_h^{PP})$ in the Gaussian beam migration equations (6) and (7) are the PP-wave complex amplitude and complex travel time, respectively, determined by the two beams from the source and receiver. Similarly,

$\overline{A}^{PS}(\mathbf{x}, \mathbf{p}_m^{PS}, \mathbf{p}_h^{PS})$ and $\overline{T}^{PS}(\mathbf{x}, \mathbf{p}_m^{PS}, \mathbf{p}_h^{PS})$ are the complex amplitude and complex travel time of the PS-wave, respectively.

$$\overline{T}^{PP}(\mathbf{x}, \mathbf{p}_m^{PP}, \mathbf{p}_h^{PP}) = T^P_{\mathbf{L}_m - \mathbf{x}_h}(\mathbf{x}, \mathbf{p}_s^P) + T^P_{\mathbf{L}_m + \mathbf{x}_h}(\mathbf{x}, \mathbf{p}_r^P), \quad (12)$$

$$\overline{T}^{PS}(\mathbf{x}, \mathbf{p}_m^{PS}, \mathbf{p}_h^{PS}) = T^P_{\mathbf{L}_m - \mathbf{x}_h}(\mathbf{x}, \mathbf{p}_s^P) + T^S_{\mathbf{L}_m + \mathbf{x}_h}(\mathbf{x}, \mathbf{p}_r^S). \quad (13)$$

When the beams from the source and the receiver are near the beam center point $\mathbf{L}_m$, the P-wave velocity may be used to compute the complex travel times $T^P_{\mathbf{L}_m - \mathbf{x}_h}(\mathbf{x}, \mathbf{p}_s^P)$ and $T^P_{\mathbf{L}_m + \mathbf{x}_h}(\mathbf{x}, \mathbf{p}_r^P)$ for the PP-wave image. Complex travel times $T^P_{\mathbf{L}_m - \mathbf{x}_h}(\mathbf{x}, \mathbf{p}_s^P)$ and $T^S_{\mathbf{L}_m + \mathbf{x}_h}(\mathbf{x}, \mathbf{p}_r^S)$ are computed using the P- and S-wave velocities, respectively, for the PS-wave image. Compared with the PP-wave, the PS-wave has polarity reversal problems, and the direct migration of the PS-wave seriously affects the migration result. Therefore, the polarity in the PS-wave records is used to correct the polarity in the Gaussian beam prestack depth migration.

Common-image gathers

First, common-offset gathers are extracted from common-shot gathers. Second, each common-offset gather is migrated by using the common-offset Gaussian beam prestack depth migration method. Finally, ODCIGs are easily extracted.

Using a concave model, as an example (Figure 1a), Figure 1b shows the common-offset gather with 1000 m offset. Figures 1c, 1d, and 1e show the ODCIGs at position CDP = 320 with the correct migration velocity, and with velocities 10% higher and lower than the correct velocity. Evidently, for the correct migration velocity, the events on the CIGs are flat and correctly positioned at depth but curve downward with increasing velocity and upward with decreasing velocity. In summary, the event curves on CIGs contain information from which the correct velocity can be estimated. This is the foundation for the residual curvature migration velocity analysis.

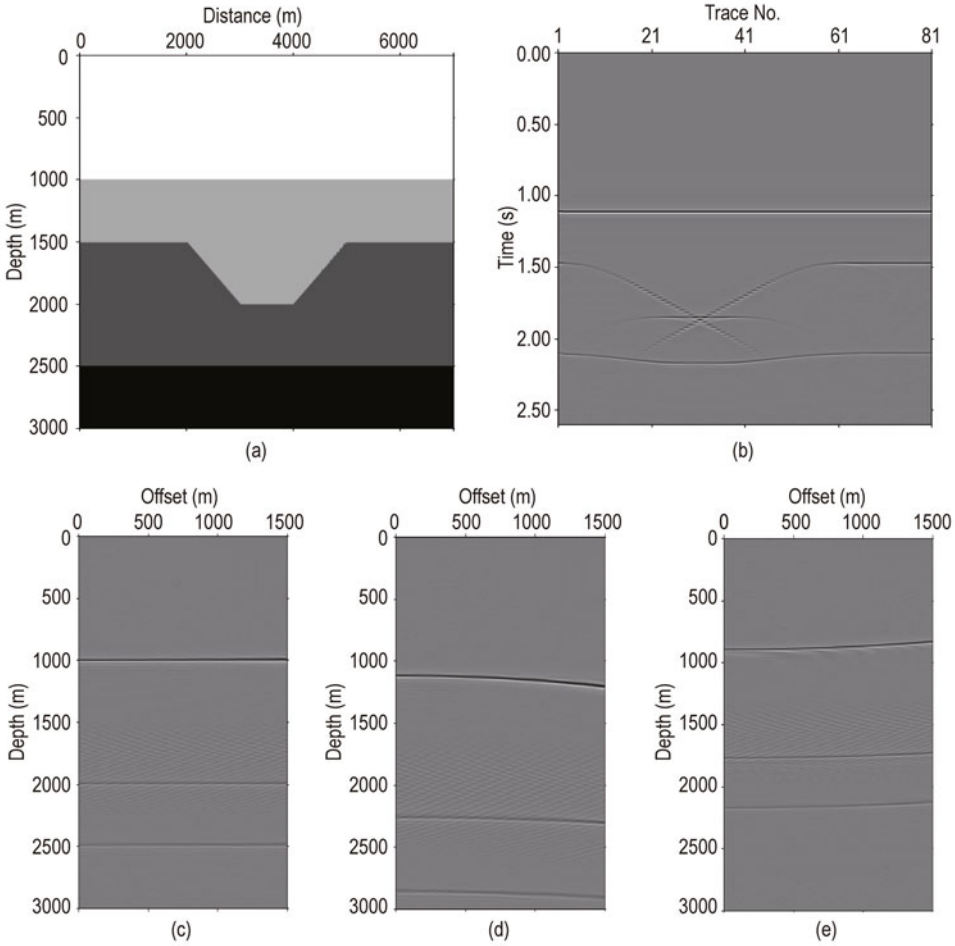

Fig.1 ODCIGs for the concave model.

(a) Velocity model, (b) Common-offset gather with 1000 m offset, (c) ODCIGs with correct migration velocity, (d) ODCIGs with 10% higher than the correct migration velocity, and (e) ODCIGs with 10% lower than the correct migration velocity.

Velocity analysis

After determining the prestack depth migration using the correct velocity, the imaged depths in a CIG must remain the same regardless of the offset. This is the basic criterion of the residual curvature velocity analysis method (Al-Yahya, 1989). Both the PP- and PS-wave migration sections are produced during multiwave migration velocity analysis, and the image depth of the target layers in the PP- and PS-wave migration sections will be consistent if P- and S-wave migration velocities are accurate. Thus, the image depth consistency principle for the PP- and PS-waves can be used to assess the correctness of the extracted velocities.

Residual depth equation

Residual curvature migration velocity analysis is based on the residual moveout in CIGs to update the velocity. Thus, it is essential to establish the relationship between the residual curvature and migration velocity.

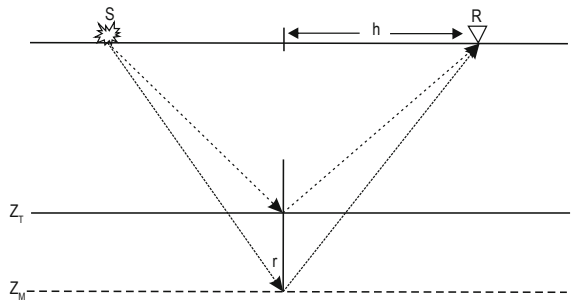

Fig.2 Sketch of P-wave propagation geometry.

We assume that the reflector is horizontal and the PP-wave geometry is that of Figure 2. We also assume that h is the half offset, y is the horizontal coordinate of the point mid-way between the source and the receiver, v_t is the true velocity, and v_m is the migration velocity. Then the image depth $z(h)$ as a function of the offset is

$$z^2(h) = \frac{v_m^2}{4} t^2(y,h) - h^2. \tag{14}$$

The true recorded travel time is

$$t^2(y,h) = t^2(y,0) + \frac{4h^2}{v_t^2}, \tag{15}$$

where t(y, 0) is the zero-offset travel time. Substituting equation (15) into equation (14), the residual depth equation of the PP-wave is

$$z^2(h) = z^2(0) + rh^2 \tag{16}$$

and

$$r = \frac{v_m^2}{v_t^2} - 1, \tag{17}$$

where $z(0)$ is the zero-offset image depth and function r describes the residual moveout, which is used to reflect the velocity error.

For a general velocity or an arbitrary reflector, the image depth as a function of the offset may be written as a Taylor series expansion (Liu, 1995)

$$z^2(h) = z^2(0) + (\frac{v_m^2}{v_t^2} - 1)h^2 + O(h^4). \tag{18}$$

Equation (18) shows that the residual-depth equation for the PP-wave for a dipping reflector is independent of the reflector dip, and the residual moveout is expressed with a hyperbolic function as in the horizontal reflector.

For the converted PS-wave, the residual depth equation resembles the PP-wave equation (Al-Zayer and Tsvankin, 2005; Maria and Robert 1998), except that r is used to describe the equivalent PS-wave velocity, as follows:

$$r = \frac{v_{ps,m}^2}{v_{ps,t}^2} - 1, \tag{19}$$

$$v_{ps,m} = \frac{2v_{p,m}v_{s,m}}{v_{p,m} + v_{s,m}}, \tag{20}$$

where $\boldsymbol{v}_{p,m}$ is the P-wave migration velocity and $\boldsymbol{v}_{s,m}$ is the S-wave migration velocity. The migration velocity analysis procedure is the same as for the PP- and PS-waves. The equivalent PS-wave velocity $\boldsymbol{v}_{ps,m}$ is obtained by PS-wave migration velocity analysis. Then, the S-wave velocity is derived.

Because it is difficult to visually judge whether the events in CIGs have been flattened, we choose the residual velocity from semblance spectra to update the velocity and then use the CIG semblance peak position to judge whether the velocity is acceptable. In this study, the layer-stripping method was used to update the velocity, that is, we start with the first layer (Liu, 1994). Once the first layer is fixed then the velocity is updated iteratively for the following layers in a top-down procedure using the residual curvature velocity analysis method.

Depth image-matching method

If the P- and S-wave migration velocities were accurate, the events in CIGs would be flattened and the image depth of the same layer in the PP- and PS-wave migration sections would be consistent. Because PP- and PS-waves migration velocity analyses are performed separately, the image depth between two migration sections may appear partially inconsistent; therefore, the velocity model must be adjusted to maintain depth matching. The process of updating the P-velocity is independent, whereas the process for updating the S-velocity depends upon the P-velocity. The signal-to-noise ratio (SNR) of the P-wave data is typically high; hence, the precision of the P-wave velocity model is considered higher than that of the S-wave velocity model. To ensure that the PP- and PS-wave images maintain a consistent depth (Sahai and Meek, 2003), the S-wave velocity model must be modified according to the following equations

$$v_{sc} = z_c /(z_i / v_{si} - \Delta z / v_p), \tag{21}$$

$$\Delta z = z_c - z_i, \tag{22}$$

where z_c is the thickness of the layer in the P-wave velocity model, assumed to have the correct thickness, z_i is the thickness of the layer after migration of the PS-wave data, which is considered to have incorrect thickness, Δz is the depth error, v_p is the P-wave velocity of the layer, v_{si} is the S-wave migration velocity of the layer, and v_{sc} is the correct S-wave velocity of the layer.

Migration velocity analysis procedure

To conduct a multiwave Gaussian beam migration velocity analysis, PP-wave data are first processed to obtain an accurate P-wave velocity model, and then, the PS-wave migration velocity is analyzed to obtain the S-wave velocity. The specific procedure is as follows:

(1) Establish the initial velocity model using velocity analysis in common scatter point gathers (Wang et al., 2012a, 2012b).

(2) Extract ODCIGs using the Gaussian beam prestack depth migration method.

(3) Calculate the semblance spectra and select the residual velocity.

(4) Update the velocity using the residual velocity.

(5) Repeat steps (2) to (4) until the velocity is accurate.

When the image depth of the same layer in the PP- and PS-wave migration sections appears inconsistent, the S-wave velocity model is modified to maintain depth matching and obtain accurate P- and S-wave velocities.

Numerical example

To verify the accuracy of the proposed multiwave Gaussian beam migration velocity analysis method, we tested it on the multilayer model shown in Figure 3. Synthetic seismograms were generated by the elastic finite-difference method, simulating 97 shots at the surface and 321 receivers per shot. In the model, the shot spacing was 50 m, and the receiver spacing was 10 m. The travel time was 3.2 s, and the sampling interval was 2 ms. We chose a control point at 3800 m from the origin (the vertical line in Figure 3) to illustrate the multiwave migration velocity analysis process.

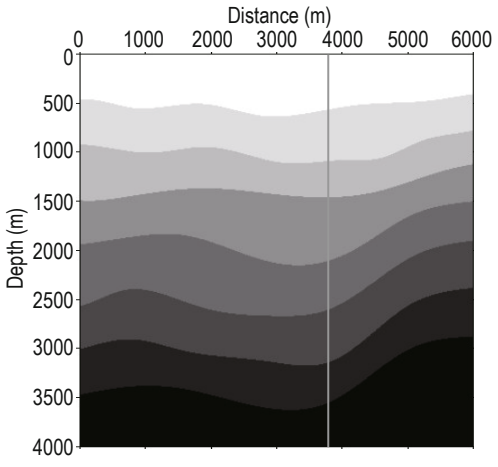

Fig.3 Multi-layer model.

Figures 4a and 4b show the initial PP- and PS-wave ODCIGs. The corresponding PP- and PS-wave CIGs semblance spectra profiles are shown in Figures 4c and 4d. The plot of events shows an upward curve in both CIGs, and the residual velocity $r < 0$ is shown in both semblance spectra profiles. This indicates that the initial P- and S-wave migration velocities are lower than the true velocities. Figures 5a and 5b are the initial PP- and PS-wave migration sections. Because the initial velocities are not accurate, the reflector images are in the wrong position. The imaged depths are shallower than the true positions. The maximum depth error was 260 m at the control point. Figure 6 shows the PP- and PS-wave ODCIGs obtained using the updated velocities and corresponding semblance spectra profiles, where the events in both CIGs are flat and the residual velocity $r = 0$ is shown in both semblance spectra profiles. Figure 7

compares the updated P- and S-wave velocities and the true P- and S-wave velocities at the control point. The maximum error in the P-wave velocity is <1%, and the maximum error in the S-wave velocity is <1.6%. Figures 8a and 8b show the final PP- and PS-wave Gaussian beam migration sections using the updated P- and S-wave

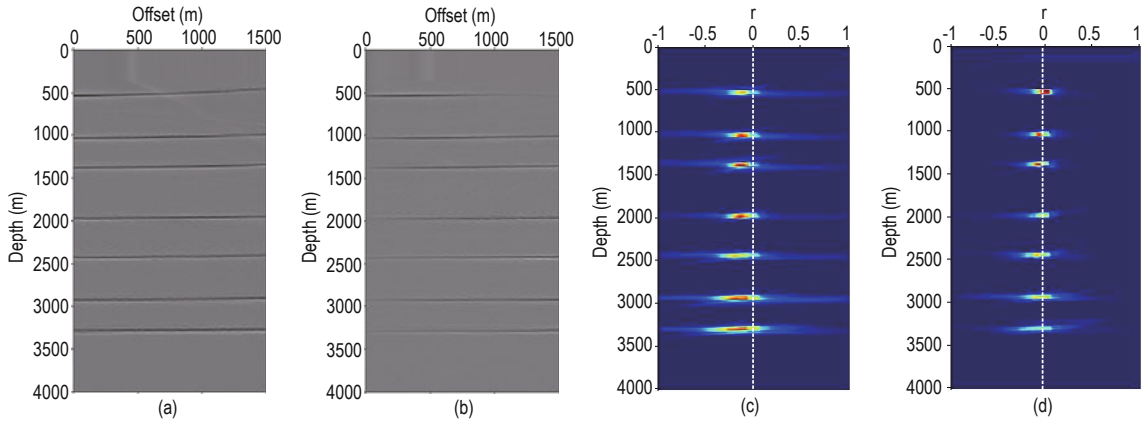

Fig.4 Initial ODCIGs at 3800 m (Figure 3 for location) and corresponding semblance spectra.

(a) PP-wave ODCIGs, (b) PS-wave ODCIGs, (c) PP-wave semblance spectra profile, and (d) PS-wave semblance spectra profile. The events curve upward and r < 0, which means that the initial migration velocities were lower than the correct values.

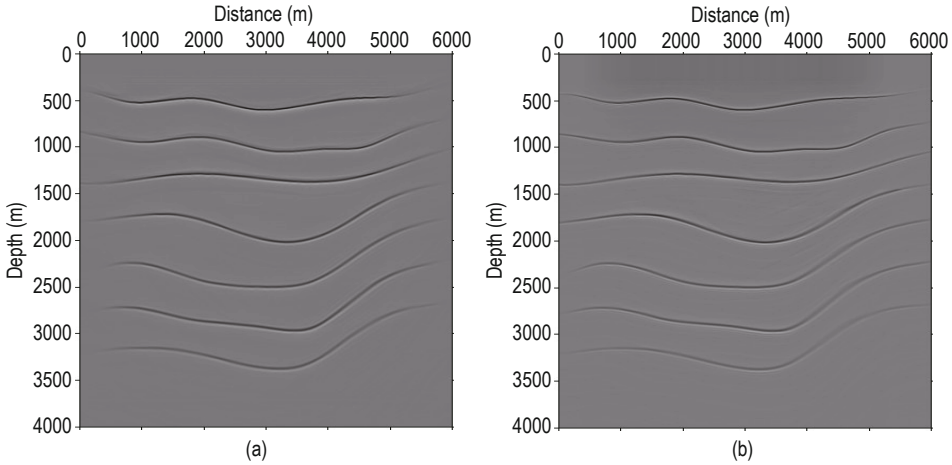

Fig.5 Initial migration sections using Gaussian beam migration with initial velocities.

(a) PP-wave and (b) PS-wave. The images are incorrect.

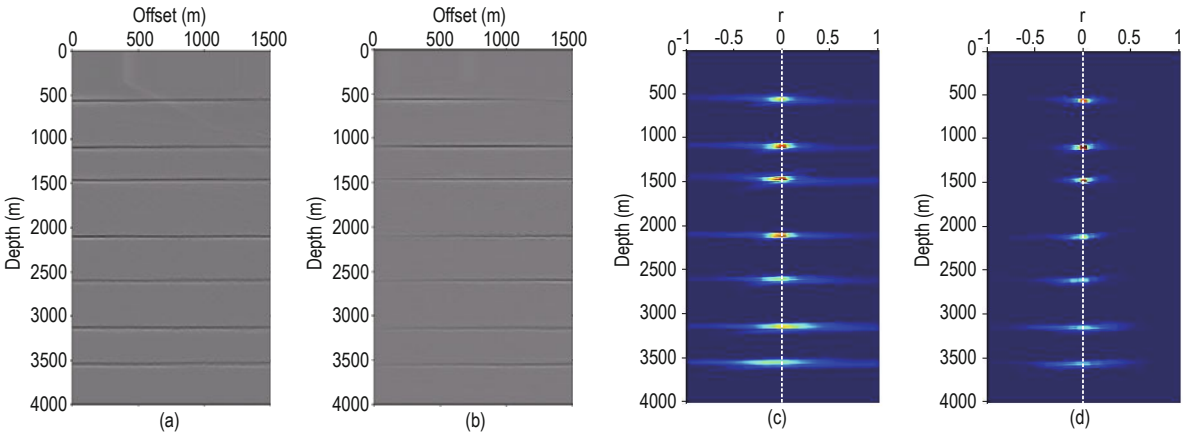

Fig.6 Updated ODCIGs obtained using the updated velocities at location 3800 m and corresponding semblance spectra.

(a) PP-wave ODCIGs, (b) PS-wave ODCIGs, (c) PP-wave semblance spectra profile, and (d) PS-wave semblance spectra profile. The events in both CIGs are flat and $r = 0$.

velocities. Both sections show the accurate images and the image depths of the PP- and PS-waves are consistent. The results verify that the proposed multiwave migration velocity analysis method is accurate.

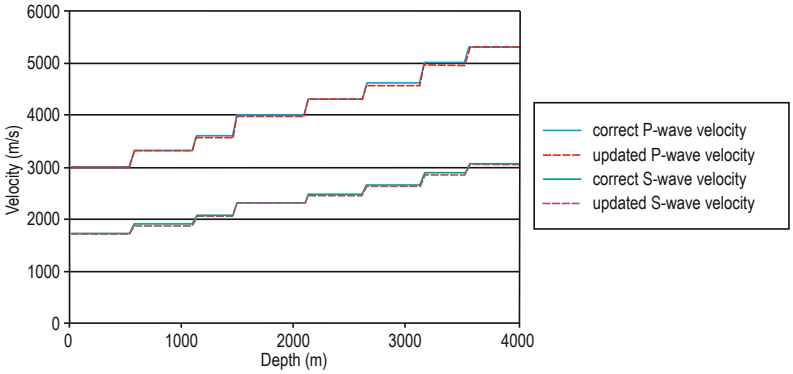

Fig.7 Comparison between the updated P- and S-wave velocities and true P- and S-wave velocities at the control point.

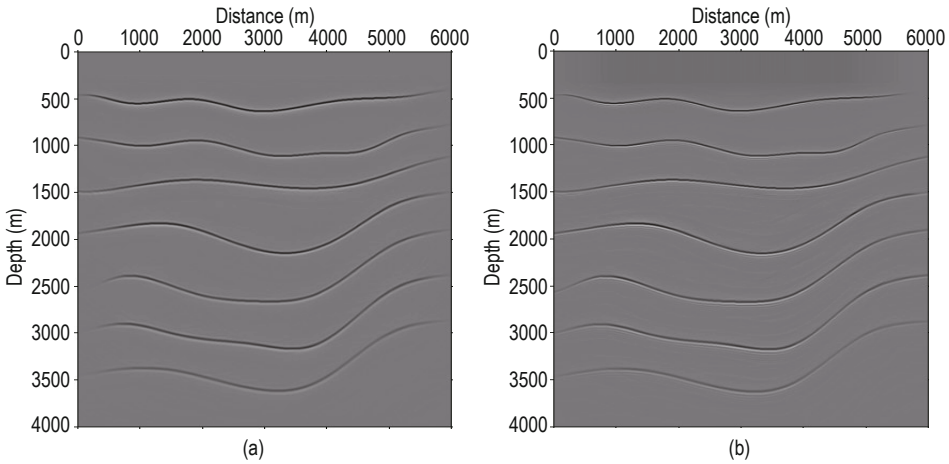

Fig.8 Final Gaussian beam migration sections using the updated velocities.
(a) PP-wave and (b) PS-wave.

Field data example

To demonstrate the applicability of the method, it was applied to a multiwave seismic dataset from northeastern China, consisting of 210 shots with trace spacing of 25 m. The minimum offset for each shot was 400 m, and the maximum offset was 2375 m. Sampling time was 5 s at 1 ms sampling intervals. Figures 9a and 9b show three-shot records of the Z- and X-component seismic data.

We chose a control point located at 5625 m. Figures 10a and 10b show the initial PP- and PS-wave ODCIGs in which the events curve downward, meaning that the initial migration velocities were higher than the true velocities. The migration velocities were updated using the proposed method to obtain the revised P- and S-wave velocities. Figures 10c and 10d show that the events curve is flat for the updated PP- and PS-wave ODCIGs. Figures 11a and 11b show the final updated P- and S-wave migration velocity fields. Figures 12a and 12b show the final PP- and PS-wave Gaussian beam migration sections. Because of the low SNR of the converted wave and the poor continuity of events, and because the converted PS-wave velocity analysis relied on the P-wave, the image quality of the PS-wave was poorer than that of the PP-wave. Nevertheless, it can be seen that the PP- and PS-wave target layers (shown by the arrows) match well in the two migration sections, and the images of the structural features are identical, which suggests that the migration velocities are reasonable. The test results verify the effectiveness of the proposed method.

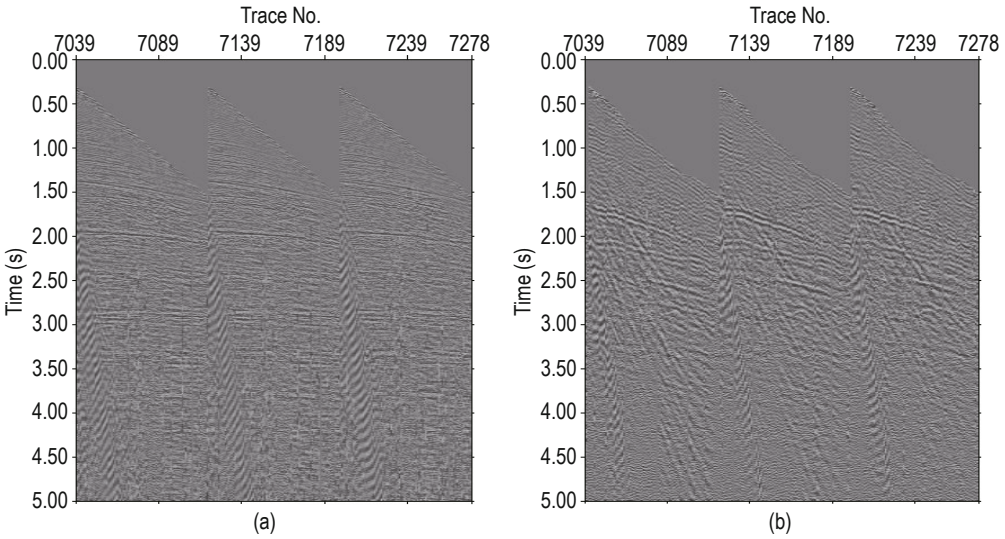

Fig.9 Field seismic records.
(a) Z-component and (b) X-component.

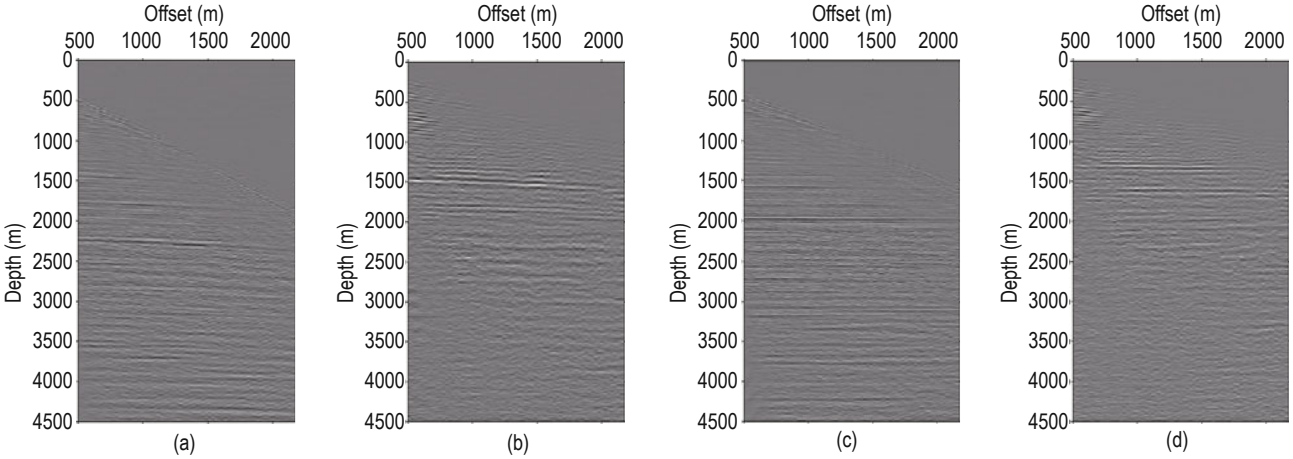

Fig.10 ODCIGs before and after migration velocity analysis.
(a) Initial PP-wave ODCIGs, (b) Initial PS-wave ODCIGs, (c) Updated PP-wave ODCIGs, and (d) Updated PS-wave ODCIGs.

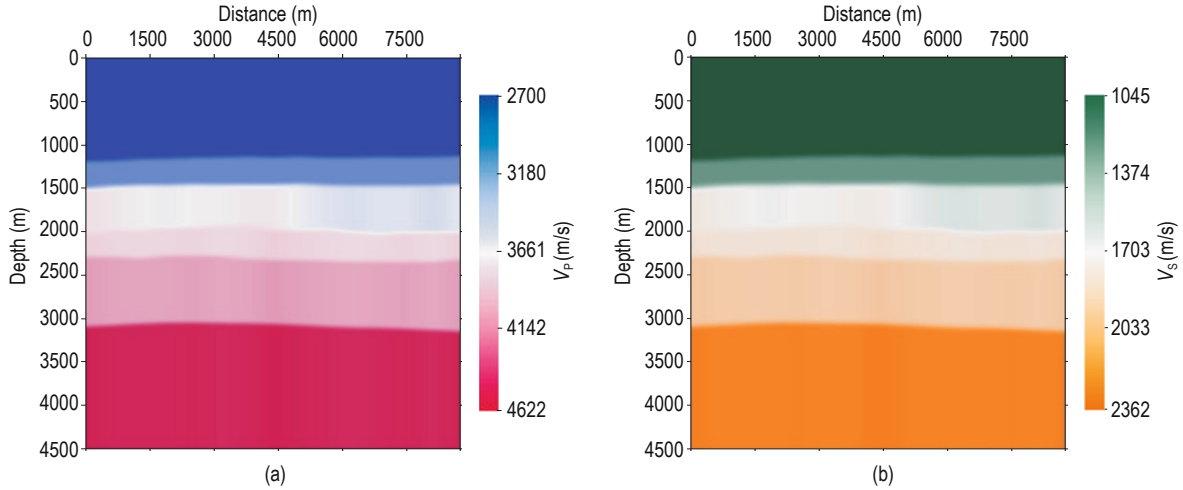

Fig.11 Final updated migration velocity fields.
(a) P-wave and (b) S-wave.

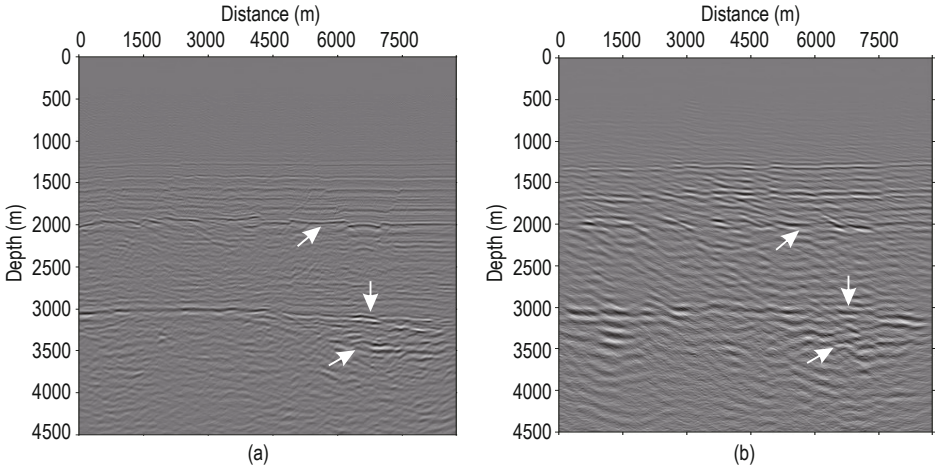

Fig.12. Final Gaussian beam migration sections.
(a) PP-wave and (b) PS-wave.

Conclusions

We have presented a multicomponent migration velocity analysis method for PP- and PS-waves based on multicomponent Gaussian beam prestack depth migration. The Gaussian beam migration is an excellent depth migration algorithm capable of solving multivalued travel times with different beams superposed. Therefore, the proposed multiwave migration velocity analysis method based on Gaussian beam migration effectively eliminates artifacts in common-image gathers due to the multivalued travel times and improves the accuracy of the migration velocity analysis. Simultaneously, the method retains the efficiency and the flexibility of the Kirchhoff migration velocity analysis method. Migration velocity models of P- and S-waves are updated based on the residual moveout in CIGs. Depending on the CIG flatness criterion and the PP- and PS-wave image depth consistency principle, accurate P- and S-wave velocities are obtained. Tests using synthetic and field seismic data show that it is an accurate and effective multicomponent migration velocity analysis method.

References

AI-Yahya, K., 1989, Velocity analysis by iterative profile migration: Geophysics, **54**(6), 718–729.

Al-Zayer, R. M., and Tsvankin, I., 2005, Image gathers of SV-waves in homogeneous and factorized VTI media: Geophysics, **70**(5), D55–D64.

Červeny, V., 1983, Synthetic body wave seismograms for laterally varying layered structures by the Gaussian beam method: Geophysical Journal of the Royal Astronomical Society, **73**, 389–426.

Červeny, V., Popov, M. M., and Psencik, I., 1982, Computation of wave fields in inhomogeneous media—Gaussian beam approach: Geophysical Journal of the Royal Astronomical Society, **70**, 109–128.

Dai, H., and Li, X. Y., 2005, Accuracy of a simplified moveout formula for PS converted-waves in multi-layered media: 75th Annual International Meeting, SEG, Expanded Abstracts, 1010–1013.

Dai, H., and Li, X. Y., 2007, Velocity model updating in prestack Kirchhoff time migration for PS converted waves: Part I-Theory: Geophysical Prospecting, **55**, 525–547.

Du, Q. Z., Li, F., Ba, J., Zhu, Y. T., and Hou, B., 2012, Multicomponent joint migration velocity analysis in the angle domain for PP-waves and PS-waves: Geophysics, **77**(1), U1–U13.

Gray, S. H., 2005, Gaussian beam migration of common-shot records: Geophysics, **70**(4), S71–S77.

Gray, S. H., and Bleistein, N., 2009, True-amplitude Gaussian-beam migration: Geophysics, **74**(2), S11–S23.

Hale, D., 1992a, Migration by the Kirchhoff, slant stack and Gaussian beam methods: Colorado School of Mines Center for Wave Phenomena Report 121.

Hale, D., 1992b, Computational aspects of Gaussian beam migration: Colorado School of Mines Center for Wave Phenomena Report 139.

Hill, N. R., 1990, Gaussian beam migration: Geophysics, **55**, 1416–1428.

Hill, N. R., 2001, Prestack Gaussian-beam depth

migration: Geophysics, **66**, 1240–1250.
Lafond, C. F., and Levander, A. R., 1993, Migration moveout analysis and depth focusing: Geophysics, **58**(1), 91-100.
Lee, W., and Zhang, L., 1992, Residual shot profile migration: Geophysics, **57**(6), 815–82.
Liu, Z. Y., 1995, Migration velocity analysis [D]. Colorado: Center for Wave Phenomena, Colorado School of Mines.
Liu, Z. Y., 1997, An analytical approach to migration velocity analysis: Geophysics, **62**(4), 1238–1249.
Liu, Z. Y., and Bleistein, N., 1994, Velocity analysis by perturbation: 64th Annual International Meeting, SEG, Expanded Abstracts, 1191–1194.
Liu, Z. Y., and Bleistein, N., 1995, Migration velocity analysis-theory and an iterative algorithm: Geophysics, **60**(1), 142–153.
Lu, J., Wang, Y., and Yao, C., 2012, Separating P- and S-waves in an affine coordinate system: Journal of Geophysics and Engineering, **9**, 12–18.
Maria, D., and Robert, R. S., 1998, Migration velocity analysis by perturbation for converted waves: CREWES Research Report, **10**(28).
Nowack, R. L., 2003, Calculation of synthetic seismograms with Gaussian beams: Pure and Applied Geophysics, **160**, 487–507.
Nowack, R. L., Chen, W. P., and Tseng, T. L., 2010, Application of Gaussian-beam migration to multiscale imaging of the lithosphere beneath the Hi-CLIMB array in Tibet: Bulletin of the Seismological Society of America, **100**(4), 1743–1754.
Nowack, R. L., Dasgupta, S., Schuster, G. T., and Sheng, J. M., 2006, Correlation migration using Gaussian beams of scattered teleseismic body waves: Bulletin of the Seismological Society of America, **96**(1), 1–10.
Nowack, R. L., Wang, C. P., Kruse, U., and Dasgupta, S., 2007, Imaging offsets in the Moho: Synthetic tests using Gaussian Beams with teleseismic waves: Pure and Applied Geophysics, **164**, 1921–1936.
Popov, M. M., Semtchenok, N. M., Popov, P. M., and Verdel, A. R., 2010, Depth migration by the Gaussian beam summation method: Geophysics, **75**(2), S81–S93.
Sahai, S. K., and Meek, R. A., 2003, S-wave velocity model building and updating for depth migration of converted wave data: 73th Annual International Meeting, SEG, Expanded Abstracts.
Sava, P., and Biondi, B., 2004a, Wave-equation migration velocity analysis-I: Theory: Geophysical Prospecting, **52**, 593–606.
Sava, P., and Biondi, B., 2004b, Wave-equation migration velocity analysis–II: Subsalt imaging examples: Geophysical Prospecting, **52**, 607–623.
Sava, P., Biondi, B., Etgen, J., 2005, Wave-equation migration velocity analysis by focusing diffractions and reflections: Geophysics, **70**(3), U19–U27.
Wang, Y., Wang, W., and Yin, J. J., 2012a, A modified EOM method for PS-wave migration: Exploration Geophysics, **43**, 156–161.
Wang, W., Wang, Y., Yin, J. J., and Gao, X., 2012b, Error analysis of the converted wave deduced by equivalent velocity assumption: Exploration Geophysics, **43**, 162–170.
Yan, J., and Sava, P., 2010, Analysis of converted-wave extended images for migration velocity analysis: 80th Annual International Meeting, SEG, Expanded Abstracts, 1666–1671.

Han Jian-Guang is a PhD student at the Institute of Geology and Geophysics, Chinese Academy of Sciences. He works for the Seismic Anisotropy, Multi-wave, and Multi-component Seismic Technique Research Group. His research work is mainly focused on the multi-component seismic imaging method.